

Performance of low-rank approximations in tensor train format (TT-SVD) for large dense tensors

Melven Röhrig-Zöllner Jonas Thies Achim Basermann

February 2, 2021

Abstract

There are several factorizations of multi-dimensional tensors into lower-dimensional components, known as ‘tensor networks’. We consider the popular ‘tensor-train’ (TT) format and ask, how efficiently can we compute a low-rank approximation from a full tensor on current multi-core CPUs.

Compared to sparse and dense linear algebra, there are much fewer and less extensive well-optimized kernel libraries for multi-linear algebra. Linear algebra libraries like BLAS and LAPACK may provide the required operations in principle, but often at the cost of additional data movements for rearranging memory layouts. Furthermore, these libraries are typically optimized for the compute-bound case (e.g. square matrix operations) whereas low-rank tensor decompositions lead to memory bandwidth limited operations.

We propose a ‘tensor-train singular value decomposition’ (TT-SVD) algorithm based on two building blocks: a ‘Q-less tall-skinny QR’ factorization, and a fused tall-skinny matrix-matrix multiplication and reshape operation. We analyze the performance of the resulting TT-SVD algorithm using the Roofline performance model. In addition, we present performance results for different algorithmic variants for shared-memory as well as distributed-memory architectures. Our experiments show that commonly used TT-SVD implementations suffer severe performance penalties. We conclude that a dedicated library for tensor factorization kernels would benefit the community: Computing a low-rank approximation can be as cheap as reading the data twice from main memory. As a consequence, an implementation that achieves realistic performance will move the limit at which one has to resort to randomized methods that only process part of the data.

1 Introduction

The tensor train (TT) decomposition is a particular form of a tensor network representation of a high-dimensional tensor in which the k 3D ‘tensor cores’ are aligned in a 1D format and connected by a contraction with their direct neighbors only to represent (or approximate) a k -dimensional tensor. It was introduced as such by Oseledets [33,35]), but in fact has been known to (and used by) theoretical physicists under the name of Matrix Product States (MPS) since the 1980s [1, 2]; see also [41] for a more recent reference. Closely related is the Density Matrix Renormalization Group (DMRG) algorithm [42], an optimization method that operates on the space of MPS. A nice overview on numerical algorithms based on low-rank tensor approximations can be found in [20]. Recent research also focuses on applications of tensor trains in data science, see e.g. [10, 11, 27, 29] for a few examples. The performance of common arithmetic operations in tensor train format (such as additions and scalar products) are discussed in [13].

One can construct an approximate TT-decomposition of high-dimensional data $X \in \mathbb{R}^{n_1 \times n_2 \times \dots \times n_d}$ using a high order singular value decomposition (HOSVD). An algorithm for the HOSVD in TT format, called TT-SVD, is presented in [34]. Given X and a maximum ‘bond dimension’ r_{max} , it successively determines the tensor cores $Y^{(j)} \in \mathbb{R}^{r_{j-1,j} \times n_j \times r_{j,j+1}}$, $j = 1 \dots d$, such that $r_{0,1} = r_{d,d+1} = 0$, $r_{i,j} < r_{max}$, the rows or columns of some matricization of all but one $Y^{(j)}$ are orthonormal, and the approximation error (difference between the tensor train formed by the $Y^{(j)}$ and the original data tensor X) is minimized (up to a constant factor) in the Frobenius norm on the manifold of rank- r_{max} tensor trains [34]. Definitions of some of these concepts are obviously needed, and will be given in Section 2.

The aim of this paper is to develop an efficient formulation and implementation of this algorithm for modern multi-core CPUs. To be more specific about our goals, we distinguish four categories of approximation problems, based on the characteristics of the data X .

1. There is too much data to be processed as a whole considering time and resource constraints, but we want to try to reveal some underlying principles. Successful methods are based on randomly choosing columns/rows/parts of the matrix/tensor, see [28, 30]. In this case, a posteriori stochastic error bounds for the approximation may be found i.e., bounds that hold with a certain probability but depend on statistical properties of the input that cannot be known without solving the deterministic least squares problem first [30].
2. The data is implicitly given by some high-dimensional function i.e., we can evaluate individual values at arbitrary positions efficiently. For this case, black-box approximation methods can be employed with (approximate) a posteriori error bounds, see [4, 32]. These methods work best if the data is known to be representable with given low rank, or is known to have quickly decreasing singular values in the desired low rank tensor format. This approach is also based on (randomly) choosing some evaluation points and strives for an approximation with as few evaluations as possible. Obviously, optimized methods for both 1 and 2 do not work if the data contains rare but significant outliers, as it would be pure luck to find it when only randomly considering a part of the data. This is formalized in [30, Theorem 3.6], which links the likely number of samples required for an ϵ -accurate least-squares approximation to the sampling probability and relative importance of matrix rows (‘leverage scores’).
3. The data is large and sparse, and it is feasible to read it at least once or twice: For this case, a practical fast implementation should exploit the known sparsity pattern, respectively the characteristics of the sparse data format. In principle, one can apply similar algorithms to those discussed in this paper. However, the difficulty arises that with each step of the TT-SVD algorithm the data usually becomes more dense.

4. The data is large and dense and it is feasible to read all data at least once or twice. This is the case we discuss in this paper. Error bounds and asymptotic complexity estimates (for the size of the result) exist but differ slightly depending on the desired tensor format, see [20] and the references therein. So one usually seeks an approximation with a specific accuracy (in terms of maximal size of the resulting approximation or a tolerance, or both). However, common implementations often provide sub-optimal performance for this case as they do not acknowledge that the problem is limited by data transfers on current computers (see Section 5).

We focus on the TT-SVD because this is a simple and popular choice. The ideas can be transferred to other tree tensor networks (see e.g. [19]) as the algorithmic building blocks are similar. An important ingredient in our implementation is a Q-less ‘tall and skinny QR’ (TSQR, see [14]) variant that is described in detail in Section 3.2. The idea to avoid computing and storing the large matrix Q of a QR decomposition was already exploited for e.g. sparse matrix decompositions and tensor calculus in [7, 17].

Our contribution is twofold. First, based on the example of the TT-SVD algorithm we show that low-rank tensor approximation is a memory-bound problem in high dimensions (in contrast to the SVD in two dimensions for square matrices). Second, we discuss how the TT-SVD algorithm can be implemented efficiently on current hardware. To underline our findings, we present performance results for the required building blocks and for different TT-SVD variants and implementations on a small CPU cluster.

The remainder of this paper is organized as follows. In Section 2, we introduce the basic concepts and notation for tensor networks and performance engineering that we will use to describe our algorithms and implementation. In Section 3 we describe the TT-SVD algorithm with focus on our tailored Q-less TSQR variant. In Section 4 we present a performance model for the two key components of TT-SVD (Q-less TSQR and a ‘tall and skinny’ matrix-matrix multiplication), as well as the overall algorithm. Numerical experiments comparing actual implementations of TT-SVD (including our own optimized version) against the performance model can be found in Section 5, and the paper closes with a summary of our findings in Section 6.

2 Background and notation

2.1 Tensor notation and operations

Classical linear algebra considers matrices and vectors ($n \times 1$ matrices) and provides a notation for operations between them based on matrix-matrix products and matrix transpositions. We make use of this common notation where possible. In this paper, a dense d -dimensional array or tensor is denoted by

$$X \in \mathbf{R}^{n_1 \times \dots \times n_d}. \quad (1)$$

We can combine and split dimensions through reshape operations:

$$Y = \text{reshape}(X, (n_1 \quad \frac{\bar{n}}{n_1 n_d} \quad n_d)) \in \mathbf{R}^{n_1 \times \bar{n}/(n_1 n_d) \times n_d}, \quad \text{with } \bar{n} := \prod_{i=1}^d n_i,$$

$$X = \text{reshape}(Y, (n_1 \quad \dots \quad n_d)). \quad (2)$$

This assumes that the dimensions of a tensor are ordered and provides a notation for folding a tensor into a matrix (matricization) and unfolding it back into a tensor. It only allows us

to combine neighboring dimensions, which is sufficient for all cases in this paper. In practice, many tensor algorithms can be written as series of matrix-operations of different matricizations of tensors, but more general reshape operations can often be implemented without overhead by just reinterpreting the data in memory (assuming an appropriate memory layout). A set of tensors and contractions between them can be visualized in a tensor network diagram, as introduced by Penrose in 1971 [36]. We use this notation to describe different variants of the TT-SVD algorithm. Details are explained in Appendix A.

2.1.1 Matrix decompositions

Tensor decompositions generalize matrix decompositions for higher dimensions. Most common variants extend the idea of the singular value decomposition of a possibly rectangular matrix $M \in \mathbf{R}^{n_1 \times n_2}$:

$$M = U\Sigma V^T \tag{3}$$

Here, $U \in \mathbf{R}^{n_1 \times r}$ and $V \in \mathbf{R}^{n_2 \times r}$ are orthogonal matrices ($U^T U = V^T V = I$) and $\Sigma = \text{diag}(\sigma_1, \dots, \sigma_r)$ is the diagonal matrix of singular values with $\sigma_1 \geq \sigma_2 \geq \dots \geq \sigma_r > 0$. The rank of the matrix is denoted by $r \leq \min(n_1, n_2)$.

In the steps of the TT-SVD algorithm, we also use the QR-decomposition

$$M = QR, \tag{4}$$

with an orthogonal matrix $Q \in \mathbf{R}^{n_1 \times n_2}$, $Q^T Q = I$ and an upper triangular matrix $R \in \mathbf{R}^{n_2 \times n_2}$ and usually $n_1 \geq n_2$.

2.2 Performance characteristics on current hardware

Current supercomputers consist of a set of compute nodes that are connected by a network (see e.g. [22]). Each compute node has one or several multi-core CPU sockets with dedicated memory. The CPU cores can access the memory of the complete node but accesses to the dedicated memory of the socket are faster (ccNUMA architecture). In addition, many supercomputers contain one or several accelerators per node, such as GPGPUs. As accelerator (device) memory is usually much smaller than the CPU (main) memory, it might not be beneficial to use accelerators for the algorithms discussed in this paper (this would require additional data transfers between accelerator and CPU memory). Therefore, we focus on the performance of modern CPU systems, but many arguments are valid for GPGPUs as well. For the performance modeling, we concentrate on the node-level performance of the required algorithmic building blocks. However, we also show results with a distributed memory variant of the TT-SVD algorithm that allows scaling beyond a single socket or node. In the implementation of the algorithms, we use OpenMP for parallelizing over the cores of one socket, and MPI for communicating between sockets and nodes. This avoids performance problems due to ccNUMA effects (accessing memory of other CPU sockets in one node).

For two decades, there has been an increasing gap between the memory bandwidth and the floating point performance, and this trend will most likely continue. To alleviate this problem, modern CPUs feature multiple levels of caches, from a small and fast cache per core (L1 cache) to larger and slower caches (usually L2 and L3), possibly shared between cores. Efficient algorithms need to exploit spatial and temporal locality (accessing memory addresses close to each other and accessing the same memory address multiple times). In addition, the floating point performance increased due to specialized wider SIMD units as well as optimized out-of-order execution of

pipelined instructions. So algorithms can only achieve high performance if they contain lots of independent instructions for contiguous chunks of data (e.g. no data dependencies and no conditional branches in the innermost loop).

The actual run-time of a program on a specific hardware may be determined by many factors. Therefore, it is helpful to model the performance based on a few simple characteristics that are anticipated to be potential bottlenecks. For our numerical application, we use the Roofline performance model [43], which considers two limiting factors. The algorithm is either compute-bound (limited by the floating point rate) or bandwidth-bound (limited by data transfers). The upper bound for the performance is thus given by

$$P_{\text{Roofline}} = \min(P_{\text{max}}, I_c b_s). \quad (5)$$

Here P_{max} and b_s characterize the hardware: P_{max} denotes the applicable peak performance. That is, the maximal performance possible when executing the required floating point operations. b_s is the obtainable bandwidth on the slowest data path (e.g. from the cache or memory that is large enough to contain all data). The bandwidth depends on the access pattern, so we need to measure it with a micro-benchmark that reflects the access pattern of the algorithm, see Table 1. The algorithm is characterized by its compute intensity I_c , which specifies the number of floating point operations per transferred byte. Of course, the Roofline model is a simplification: in particular, it assumes that data transfers and calculations overlap, which is not realistic if the compute intensity is close to P_{max}/b_s . However, the model provides insight into the behavior of the algorithm, and it allows us to assess if a specific implementation achieves a reasonable fraction of the possible performance.

To analyze an algorithm in this paper, we usually first estimate the compute intensity I_c and decide whether the algorithm is compute-bound or memory-bound (limited by main memory bandwidth) on the given hardware.

$$I_c \approx \frac{n_{\text{flops}}}{V_{\text{read}} + V_{\text{write}}}. \quad (6)$$

Then, we calculate the ideal run-time t_{min} from the number of floating point operations n_{flops} , respectively from the main memory data transfer volume $V_{\text{read}} + V_{\text{write}}$:

$$I_c > \frac{P_{\text{max}}}{b_s} \quad \Rightarrow \quad t_{\text{min}} = \frac{n_{\text{flops}}}{P_{\text{max}}} \quad (\text{compute-bound}) \quad (7)$$

$$I_c < \frac{P_{\text{max}}}{b_s} \quad \Rightarrow \quad t_{\text{min}} = \frac{V_{\text{read}} + V_{\text{write}}}{b_s} \quad (\text{memory-bound}) \quad (8)$$

Characteristic values for the peak floating point performance and different bandwidths can be found in Table 1. For the hardware used in our experiments, we have $\frac{P_{\text{max}}}{b_s} \approx 10$.

3 Algorithm

In this section we discuss different variants of the TT-SVD algorithm from [34]. We focus on algorithmic choices required for an efficient implementation on current hardware that retains numerical accuracy and robustness. As an important building block, we present a Q-less rank-preserving QR implementation for tall-skinny matrices (Q-less TSQR) based on [15].

3.1 TT-SVD

Based on the original TT format [34], several other formats have been suggested, such as the QTT format (see e.g. [26] and the references therein), and the QTT-Tucker format [16]. These formats

have interesting numerical properties, however, the required steps for calculating a high-order SVD from dense data in these formats are similar. For simplicity, we describe the algorithm for the TT format, although it is important that the individual dimensions are as small as possible (e.g. two as in the QTT format) to obtain high performance. For other hierarchical formats such as the \mathcal{H} -Tucker format (see e.g. [19]), the rank is defined differently, so the complexity analysis of the algorithm is specific to the (Q)TT format. The algorithmic principles and required building blocks still remain similar for HOSVD algorithms for other tree tensor network formats.

3.1.1 Original TT-SVD algorithm

We first show how the original TT-SVD algorithm from [34] can be implemented. For ease of notation, we start with dimension n_d (right-most tensor core in the TT-format):

Input: $X \in \mathbf{R}^{n_1 \times \dots \times n_d}$, max. TT-rank $r_{\max} \geq 1$, tolerance ϵ

Output: $T_1 \odot \dots \odot T_d \approx X$, $T_i \in \mathbf{R}^{r_{i-1} \times n_i \times r_i}$ with $r_0 = r_d = 1$

(where $T_1 \odot T_2$ is a contraction between the last dimension of T_1 and the first dimension of T_2)

- 1: $\bar{n} \leftarrow \prod_{i=1}^d n_i$
- 2: $r_d \leftarrow 1$
- 3: **for** $i = d, \dots, 2$ **do**
- 4: $X \leftarrow \text{reshape}(X, (\frac{\bar{n}}{n_i r_i} \quad n_i r_i))$
- 5: Calculate SVD: $U \Sigma V^T = X$ with $\Sigma = \text{diag}(\sigma_1, \dots, \sigma_{n_i r_i})$
- 6: Choose rank $r_{i-1} = \max(\{j \in \{1, \dots, r_{\max}\} : \sigma_j \geq \epsilon \sigma_1\})$
- 7: $T_i \leftarrow \text{reshape}(V_{:,1:r_{i-1}}^T, (r_{i-1} \quad n_i \quad r_i))$
- 8: $X \leftarrow U_{:,1:r_{i-1}} \text{diag}(\sigma_1, \dots, \sigma_{r_{i-1}})$
- 9: $\bar{n} \leftarrow \frac{\bar{n} r_{i-1}}{n_i r_i}$ (new total size of X)
- 10: **end for**
- 11: $T_1 \leftarrow \text{reshape}(X, (1 \quad n_1 \quad r_1))$

The costly steps in this algorithm are computing the SVD in line 5, and evaluating the reduced matrix X for the next iteration in line 8. And, depending on the implementation, the reshape operation in line 4 might require copying or reordering the data in memory. In this algorithm, the total size \bar{n} of X is reduced in each step by a factor $\frac{r_{i-1}}{n_i r_i} \leq 1$. And X is very tall and skinny except for the last iterations, where X is much smaller due to the reduction in size \bar{n} in each step. Therefore, it is advisable to apply the QR trick for calculating the SVD:

$$\begin{aligned} X &= QR, \\ \bar{U} \Sigma V^T &= R, \quad \text{with,} \\ U &= Q \bar{U}. \end{aligned} \tag{9}$$

This idea has been discussed in the literature in similar settings, see e.g. [12], but we can exploit some specific details here.

We remark that we can also start the iteration in the middle of the tensor train by reshaping X into an (almost) square matrix of size approximately $\sqrt{\bar{n}} \times \sqrt{\bar{n}}$ and splitting it with an SVD into two independent iterations for a left and a right part. This approach is not advisable because it requires $O(\bar{n}^{\frac{3}{2}})$ operations in contrast to $O(\bar{n})$ operations for algorithms that start at the boundaries of the tensor train (see Section 4.2).

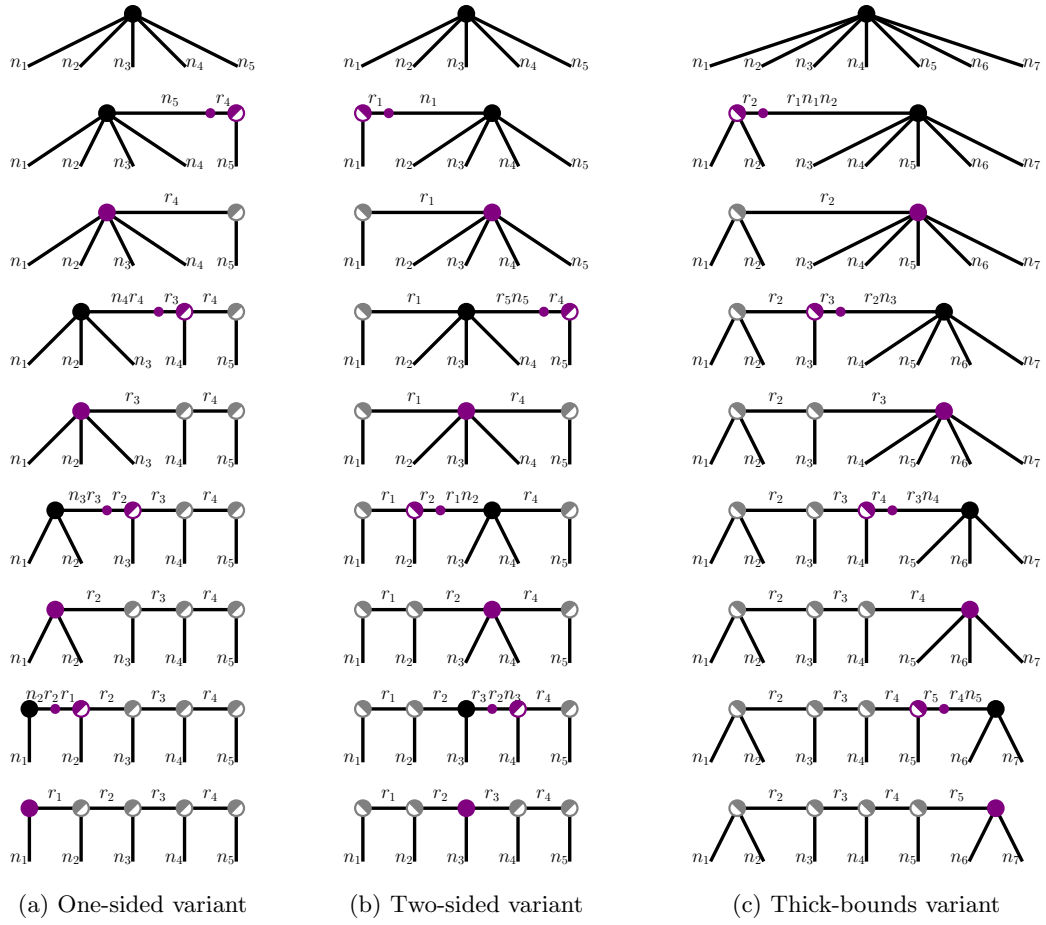


Figure 1: Graphical visualization of different TT-SVD algorithms.

3.1.2 TSQR TT-SVD algorithm

The following algorithm is based on the original TT-SVD algorithm but avoids some unnecessary computations and data transfers.

Input: $X \in \mathbf{R}^{n_1 \times \dots \times n_d}$, max. TT-rank $r_{\max} \geq 1$, tolerance ϵ

Output: $T_1 \odot \dots \odot T_d \approx X$, $T_i \in \mathbf{R}^{r_{i-1} \times n_i \times r_i}$ with $r_0 = r_d = 1$

(where $T_1 \odot T_2$ is a contraction between the last dimension of T_1 and the first dimension of T_2)

- 1: $\bar{n} \leftarrow \prod_{i=1}^d n_i$
- 2: $r_d \leftarrow 1$
- 3: $X \leftarrow \text{reshape}(X, \begin{pmatrix} \bar{n} & n_d \end{pmatrix})$ (only reinterprets data in memory)
- 4: **for** $i = d, \dots, 2$ **do**
- 5: Calculate QR decomposition: $QR = X$ (and discard Q)
- 6: Calculate small SVD: $\bar{U}\Sigma V^T = R$ with $\Sigma = \text{diag}(\sigma_1, \dots, \sigma_{n_i r_i})$
- 7: Choose rank $r_{i-1} = \max(\{j \in \{1, \dots, r_{\max}\} : \sigma_j \geq \epsilon \sigma_1\})$
- 8: $T_i \leftarrow \text{reshape}\left(V_{:,1:r_{i-1}}^T, \begin{pmatrix} r_{i-1} & n_i & r_i \end{pmatrix}\right)$
- 9: $\bar{n} \leftarrow \frac{\bar{n} r_{i-1}}{n_i r_i}$
- 10: $X \leftarrow \text{reshape}\left(XV_{:,1:r_{i-1}}, \begin{pmatrix} \bar{n} & n_{i-1} r_{i-1} \end{pmatrix}\right)$
- 11: **end for**
- 12: $T_1 \leftarrow \text{reshape}(X, \begin{pmatrix} 1 & n_1 & r_1 \end{pmatrix})$

Here, the costly operations are the tall-skinny QR decomposition in line 5 and the tall-skinny matrix-matrix product in line 10. We never compute the large matrix Q of the QR decomposition because it is faster to obtain the new X from $XV_{:,1:r_{i-1}}$ instead of calculating the matrix Q first and then evaluating $Q\bar{U}_{:,1:r_{i-1}} \text{diag}(\sigma_1, \dots, \sigma_{r_{i-1}})$. In addition, we can fuse the tall-skinny matrix-matrix product and the reshape operation but this usually requires an additional buffer (efficient in-place product+reshape is tricky due to the memory layout). So this step is implemented as

$$Y \leftarrow \text{reshape}\left(XV_{:,1:r_{i-1}}, \begin{pmatrix} \bar{n} & n_{i-1} r_{i-1} \end{pmatrix}\right)$$

$$\text{swap}(X, Y)$$

where $\text{swap}(\cdot, \cdot)$ just resets a pointer to the current data. The reshape operations require re-ordering in memory in our implementation due to padding of dimensions in the memory layout. The padding is chosen such that the stride of the leading dimension is a multiple of the SIMD width not close to a power of two to avoid cache thrashing (see e.g. [22]). This is crucial for the performance of the algorithm for the QTT case as 2^d tensors lead to bad strides in all matrix operations otherwise.

Variants Fig. 1a visualizes the TSQR TT-SVD algorithm using tensor network diagrams. We would like to briefly discuss two interesting variants of the algorithm. First, we can alternately calculate TT cores on the left and on the right (two-sided variant), see Fig. 1b. This may reduce the complexity because the TT-ranks are usually increasing from the boundaries to the center. However, our implementation requires an additional transpose operation (swapping dimensions in memory) because the TSQR implementation expects a column-major memory layout. Second, we can combine multiple dimensions on the left and right boundaries, see Fig. 1c. The idea of this approach is to achieve a significant reduction of the size of X in the first step.

3.2 Rank-preserving Q-less TSQR reduction with Householder reflections

In this section, we present the low-level building blocks for implementing a robust, highly-efficient and rank-preserving tall-skinny QR decomposition based on the communication-avoiding QR factorization in [15]. The QR decomposition is rank-preserving in the following sense: It does not break down if the input matrix is rank-deficient, and the resulting triangular matrix R has the same (numerical) rank as the input matrix. For numerical robustness, we choose an implementation based on Householder reflections [24]. As we do not need the matrix Q in any form, its data is not even stored implicitly as in common LAPACK [3] routines to reduce memory traffic. The core building block considers a rectangular matrix with zero lower left triangle W and transforms it to an upper triangular matrix R by an orthogonal transformation Q :

$$\underbrace{\begin{pmatrix} * & * & * & \cdots & * \\ \vdots & \vdots & \vdots & & \vdots \\ * & * & * & \cdots & * \\ 0 & * & * & \cdots & * \\ \vdots & & \ddots & & \vdots \\ 0 & 0 & \cdots & * & * \\ 0 & 0 & \cdots & 0 & * \end{pmatrix}}_W = Q \underbrace{\begin{pmatrix} * & * & * & \cdots & * \\ 0 & * & * & \cdots & * \\ \vdots & & \ddots & & \vdots \\ 0 & 0 & \cdots & * & * \\ 0 & 0 & \cdots & 0 & * \end{pmatrix}}_R. \quad (10)$$

With this building block, we can combine two triangular factors (without exploiting the additional zeros)

$$\begin{pmatrix} R_1 \\ R_2 \end{pmatrix} = Q_{12} R_{12}, \quad (11)$$

as well as a triangular factor and a rectangular dense matrix

$$\begin{pmatrix} M \\ R_1 \end{pmatrix} = Q_2 R_2. \quad (12)$$

These are all the required steps to setup a TSQR algorithm as described in [15]. We implemented this building block as follows:

Input: $W \in \mathbf{R}^{(n_b+m) \times m}$ with $W_{n_b+i,j} = 0 \forall i > j$ and $\epsilon_{FP} > 0$

(lower left corner of W is zero,

ϵ_{FP} is the smallest representable positive floating point number)

Output: $R \in \mathbf{R}^{m \times m}$ with $W = QR$ and $R_{i,j} = 0 \forall i > j$ and $Q^T Q = I$

(R is upper triangular, Q is only calculated implicitly and discarded)

- 1: **for** $j = 1, \dots, m$ **do**
- 2: $u \leftarrow W_{j:j+n_b,j}$
- 3: $t \leftarrow \|u\|_2^2 + \epsilon_{FP}$
- 4: $\alpha \leftarrow \sqrt{t + \epsilon_{FP}}$
- 5: **if** $u_1 > 0$ **then**
- 6: $\alpha \leftarrow \alpha \cdot (-1)$
- 7: **else**
- 8: $\alpha \leftarrow \alpha \cdot (1)$ (Required for a branch-less SIMD implementation.)
- 9: **end if**
- 10: $t \leftarrow t - \alpha u_1$

```

11:  $u_1 \leftarrow u_1 - \alpha$ 
    ( $0.5\|u - \alpha e_1\|_2^2 = 0.5\|u\|_2^2 - u_1\alpha + 0.5\alpha^2 = \|u\|_2^2 - u_1\alpha$ )
12:  $\beta \leftarrow 1/\sqrt{t}$ 
13:  $v \leftarrow \beta u$ 
14:  $W_{j:j+n_b,j} \leftarrow \alpha e_1$ 
15: for  $k = j + 1, \dots, m$  do
16:    $\gamma \leftarrow v^T W_{j:j+n,k}$ 
17:    $W_{j:j+n_b,k} \leftarrow W_{j:j+n_b,k} - \gamma v$ 
18: end for
19: end for
20:  $R \leftarrow W_{1:m,1:m}$ 

```

The main difference to the usual Householder QR algorithm consists of the additional term ϵ_{FP} in line 3 and line 4. The reflection is still numerically robust through the choice of the sign of α in lines 5 to 9: in line 10 and line 11, we obtain $t > 0$ and $\alpha u_1 \leq 0$ so that there is no cancellation. In addition, by adding $\epsilon_{FP} > 0$, we ensure that the algorithm cannot break down (no division by zero in line 12 as $t \geq \sqrt{\epsilon_{FP}}$). For $\|u\|_2 = 0$ the algorithm results in:

$$\begin{aligned}
t &= \epsilon_{FP}, \\
\alpha &= \sqrt{2\epsilon_{FP}}, \\
u_1 &= -\alpha = -\sqrt{2\epsilon_{FP}}, \\
\beta &= \frac{1}{\sqrt{t}} = \frac{1}{\sqrt{\epsilon_{FP}}} \\
\Rightarrow v &= e_1 \beta u_1 = -\sqrt{2} e_1.
\end{aligned} \tag{13}$$

So for a zero column at some point in the calculation, we obtain the Householder reflector $I - 2e_1 e_1^T$. For almost zero $\|u\|_2^2$, the calculated vector v still has norm $\sqrt{2}$ which makes $I - vv^T$ a Householder reflector (with $w = W_{j:j+n_b,j}$):

$$\|v\|_2^2 = \frac{\|w - \alpha e_1\|_2^2}{\|w\|_2^2 + \epsilon_{FP} - w_1 \alpha} = \frac{\|w\|_2^2 - 2\alpha w_1 + \alpha^2}{\|w\|_2^2 + \epsilon_{FP} - w_1 \alpha}. \tag{14}$$

With $\alpha^2 = \|w\|_2^2 + 2\epsilon_{FP}$, this yields:

$$\|v\|_2^2 = \frac{\|w\|_2^2 - 2\alpha w_1 + \|w\|_2^2 + 2\epsilon_{FP}}{\|w\|_2^2 + \epsilon_{FP} - w_1 \alpha} = 2. \tag{15}$$

We can implement this modified algorithm very efficiently on current hardware: All operations are fully independent of the actual data as there is no pivoting and the conditional sign flip in line 6 can be transformed to floating point instructions. Moreover, all operations use the same vector length n which can be a multiple of the SIMD width of the system. For a larger number of columns m (e.g. 50 or 100 in our experiments), applying the Householder reflections becomes more and more costly (lines 15 to 18 with a run-time complexity of $O(n_b m^2)$). We can perform loop unrolling and blocking to increase the performance by storing multiple reflection vectors in a buffer and applying them at once. Based on the Householder QR reduction step, we implemented a hybrid-parallel (MPI+OpenMP) communication-avoiding TSQR scheme (see [15] for more details on TSQR).

4 Performance analysis

In this section we first analyze the performance of the building blocks and then model the runtime of the complete TT-SVD algorithm. We assume that the dense input tensor is stored in main memory. If we read the input data from disc, the same principles apply but the gap between bandwidth and floating point performance is even larger.

4.1 Building blocks

4.1.1 Q-less TSQR algorithm

For $X \in \mathbf{R}^{n \times m}$ with $n \gg m$, the TSQR algorithm described in Section 3.2 calculates the triangular matrix $R \in \mathbf{R}^{m \times m}$ of the QR decomposition of X . A cache-friendly implementation only reads X once from main memory ($V_{\text{read}} = 8nm$ bytes for double-precision). Thus, a pure load benchmark shows the upper bound for the possible bandwidth $b_s = b_{\text{load}}$. We estimate the required floating point operations of the Householder QR reduction by considering the following steps in the algorithm:

```

for  $j = 1, \dots, m$  do
  (...)
   $t \leftarrow \|u\|_2^2 + \epsilon_{FP}$ 
  (...)
   $v \leftarrow \beta u$ 
  (...)
  for  $k = j + 1, \dots, m$  do
     $\gamma \leftarrow v^T W_{j:j+n_b, k}$ 
     $W_{j:j+n_b, k} \leftarrow W_{j:j+n_b, k} - \gamma v$ 
  end for
end for

```

We can simplify this to $\sum_{k=1}^m (m - k + 1) = \frac{m(m+1)}{2}$ dot products and scaled vector additions (axpy) of length $n_b + 1$. This results in $m(m+1)(n_b + 1)$ FMA (fused multiply-add) instructions, respectively $2m(m+1)(n_b + 1)$ floating point operations. We need to perform n/n_b such reduction steps assuming a flat TSQR reduction scheme. In practice, we perform some additional reduction steps with a different block size n_b depending on the number of OpenMP threads and MPI processes, but these are negligible for large n . Overall, we obtain:

$$n_{\text{flops}} \approx \frac{n}{n_b} (2m(m+1)(n_b + 1)) \approx \left(1 + \frac{1}{n_b}\right) 2nm^2 \quad (16)$$

$$\Rightarrow I_c = \frac{n_{\text{flops}}}{V_{\text{read}}} \approx \left(1 + \frac{1}{n_b}\right) \frac{m}{4}. \quad (17)$$

In the cache-friendly algorithm, we choose the block size n_b such that a matrix of size $n_b m$ fits well into the lowest level cache. The compute intensity shows that the algorithm is memory-bound for m up to ~ 50 (see Table 1 for some numbers from benchmarks).

4.1.2 Tall-skinny matrix-matrix multiplication

For $X \in \mathbf{R}^{n \times m}$, $M \in \mathbf{R}^{m \times k}$ and $Y \in \mathbf{R}^{\hat{n} \times \hat{m}}$ with $n \gg m$ and $\hat{n}\hat{m} = nk$, the fused kernel for a tall-skinny matrix-matrix multiplication and a reshape operation calculates:

$$Y \leftarrow \text{reshape}(XM, (\hat{n} \ \hat{m})) \quad (18)$$

The reshape operation just modifies the memory layout of the result and has no influence on the performance. The matrix-matrix multiplication requires $2nmk$ floating point operations and can exploit modern FMA (fused multiply-add) instructions. So we obtain $P_{\max} = P_{\text{peak}}$ as the upper limit for the performance. The operation reads X ($8nm$ bytes for double-precision) and writes Y ($8nk$ bytes) using non-temporal stores. The ratio of read to write volume is defined by m/k . In our experiments, we have $m/k \approx 2$, so we approximate the limiting bandwidth with a STREAM benchmark: $b_s = b_{\text{STREAM}}$. The resulting double-precision compute intensity is $I_c = \frac{mk}{4(m+k)} \approx \frac{m}{12}$ for $m/k \approx 2$. So on modern hardware, this operation is memory-bound for m up to ~ 150 (see Table 1).

4.2 Complete TT-SVD algorithm

For the complete TT-SVD algorithm, we first assume that the number of columns m in the required building blocks is small enough such that they operate in the memory-bound regime. So we can estimate a lower bound for the run-time by considering the data transfers in the main building blocks (Q-less TSQR algorithm and tall-skinny matrix-matrix multiplication). One TSQR TT-SVD iteration first reads the input data (TSQR step) and then reads it again and writes a reduced data set (tall-skinny matrix-matrix multiplication step). So for each iteration, we obtain

$$\begin{aligned} V_{\text{read}} &= 2\bar{n}, \\ V_{\text{write}} &= f\bar{n}, \end{aligned} \tag{19}$$

where \bar{n} denotes the total size of the input data of that iteration and $f \in (0, 1]$ the reduction factor ($\frac{r_i-1}{n_i r_i}$ in the TSQR TT-SVD algorithm). This is the lowest data transfer volume possible for one step in the TT-SVD algorithm if we assume that we need to consider all input data before we can compress it (*global* truncated SVD or QR decomposition). *Local* transformations are possible by e.g. calculating truncated SVDs of blocks of the input matrix that fit into the cache and combining them later. Such a *local* approach could at best improve the performance by roughly a factor of two as it only needs to read the data once instead of twice. However, this reduces the accuracy of the approximation (combining multiple *local* approximations instead of one *global* approximation for each step). For the complete TSQR TT-SVD algorithm, we sum up the data transfers of all iterations:

$$\begin{aligned} \bar{V}_{\text{read}} &= 2\bar{n} + 2f_1\bar{n} + 2f_1f_2\bar{n} + \dots, \\ \bar{V}_{\text{write}} &= f_1\bar{n} + f_1f_2\bar{n} + \dots \end{aligned} \tag{20}$$

Here, the coefficients f_i denote the reduction of the data size in the individual iterations. This shows that we need a significant reduction $f_1 < 1$ in the first step for optimal performance. As discussed in Section 3.1.2, we can achieve this by combining multiple dimensions such that the number of columns $m > r_{\max}$ in the TSQR step. With $\bar{f} \geq f_i$ we can estimate an upper bound for the data transfer volume of the complete algorithm:

$$\bar{V}_{\text{read}} + \bar{V}_{\text{write}} \lesssim \frac{2\bar{n}}{1-\bar{f}} + \frac{\bar{f}\bar{n}}{1-\bar{f}}. \tag{21}$$

This indicates that a very small reduction factor f_i would be beneficial. The theoretical minimum run-time amounts to the time for reading the input data twice. However, by combining dimensions to reduce $f_i \leq r_{\max}/m$ in the steps of the algorithm, the compute intensity increases and at some point the building blocks become compute-bound. For a rank-1 approximation, we

can choose a small reduction factor (e.g. $\bar{f} = 1/16$ in our implementation), resulting in an overall transfer volume of

$$\bar{V}_{\text{read}} + \bar{V}_{\text{write}} \lesssim 2.2\bar{n} \quad \text{for } \bar{f} = \frac{1}{16}. \quad (22)$$

For larger maximal rank, we use the more conservative choice $\bar{f} = 1/2$, leading to:

$$\bar{V}_{\text{read}} + \bar{V}_{\text{write}} \lesssim 5\bar{n} \quad \text{for } \bar{f} = \frac{1}{2}. \quad (23)$$

So for strongly memory-bound cases (small r_{max}), we expect a run-time in the order of copying the data once or twice in memory.

In contrast, for larger r_{max} the problem becomes more and more compute-bound. The building blocks need approximately $2nm^2$, respectively $2nmk$ floating point operations for matrices of size $n \times m$. In the individual steps of the algorithm, we have $k = r_i$ and $m = r_i/f_i$ and nm is the total size of the data:

$$n_{\text{flops}} \approx 2\bar{n} \left(\frac{r_1}{f_1} + r_1 \right) + 2\bar{n}f_1 \left(\frac{r_2}{f_2} + r_2 \right) + 2\bar{n}f_1f_2 \left(\frac{r_3}{f_3} + r_3 \right) + \dots \quad (24)$$

For $f_i \approx \bar{f}$ and $r_i \leq r_{\text{max}}$ we can estimate an upper bound for the floating point operations:

$$n_{\text{flops}} \lesssim 2\bar{n}r_{\text{max}} \left(\frac{1}{\bar{f}} + \frac{2}{1-\bar{f}} \right) \quad (25)$$

With the choice for \bar{f} from above we obtain

$$n_{\text{flops}} \lesssim 36\bar{n}r_{\text{max}} \quad \text{for } \bar{f} = \frac{1}{16}, \quad (26)$$

respectively

$$n_{\text{flops}} \lesssim 12\bar{n}r_{\text{max}} \quad \text{for } \bar{f} = \frac{1}{2}. \quad (27)$$

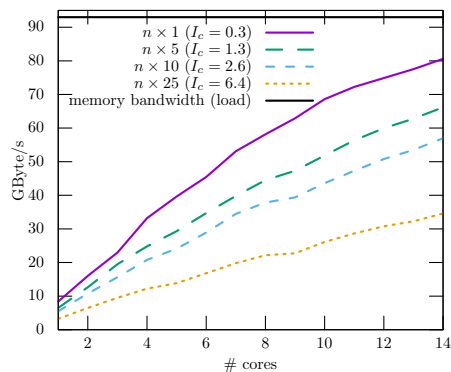
We remark that this approximation neglects the operations of the small SVD calculations of the triangular factors. So it is only valid for higher dimensions, e.g. for $\bar{n} := \prod n_i \gg (\max n_i)^3$. So for the compute-bound case, the optimal reduction factor is roughly $\bar{f} \approx 0.4$, and we expect a linear increase in run-time for increasing values of r_{max} given a fixed reduction factor \bar{f} . In addition, for large dimensions n_i the reduction factors become very small ($f_i \sim 1/n_i$) and thus the computational complexity increases.

5 Numerical experiments

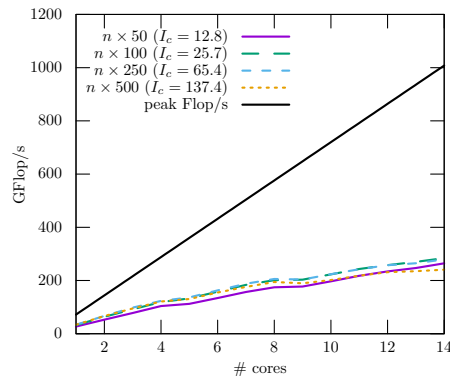
In this section, we first discuss the performance of the building blocks and then consider different variants and implementations of the complete TT-SVD algorithm. We perform all measurements on a small CPU cluster, see Table 1 for information on the hardware and its peak performance and memory bandwidth. For most of the experiments, we only use a single CPU socket of a 4-socket node to avoid any influence of NUMA effects (accessing memory from another CPU socket).

benchmark	measurement
memory bandwidth (pure load)	93 GByte/s
memory bandwidth (copy)	70 GByte/s
memory bandwidth (stream)	73 GByte/s
memory bandwidth (pure store)	45 GByte/s
double precision performance (AVX512 FMA)	1009 GFlop/s

Table 1: Hardware characteristics of a 14-core Intel Xeon Scalable Processor *Skylake* Gold 6132. The data was measured using likwid-bench [39] on a single socket of a 4-socket node. All memory benchmarks use non-temporal stores.



(a) Memory-bound case ($I_c \lesssim 11$) measured with $n = 10^7$.



(b) Compute-bound case ($I_c \gtrsim 11$) measured with $n = 5 \cdot 10^6$.

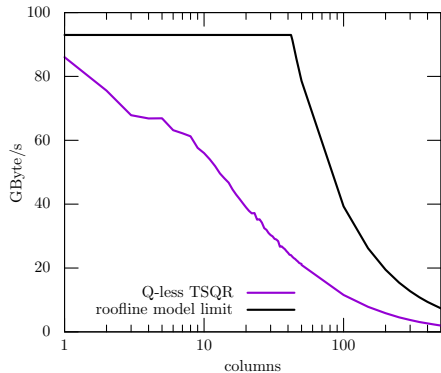
Figure 2: Single socket Q-less TSQR compared with the peak bandwidth respectively the peak Flop/s.

5.1 Building blocks

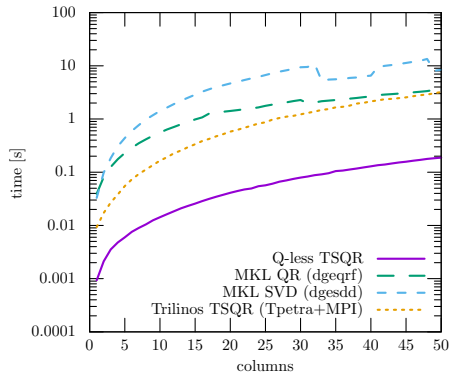
The important building blocks are the Q-less TSQR algorithm and the tall-skinny matrix-matrix multiplication (fused with a reshape of the result). Depending on the desired TT-rank in the TT-SVD algorithm, the number of columns m changes for the tall-skinny matrices in the building blocks. Therefore, we need to consider the performance for varying numbers of columns.

5.1.1 Q-less TSQR algorithm

As analyzed in Section 4.1.1, the Q-less TSQR algorithm is memory-bound for m up to ~ 50 columns on the hardware used. As we do not store the Q matrix of the tall-skinny QR decomposition, its run-time is limited by the load memory bandwidth. We expect a saturating behavior of the measured bandwidth up to the peak load bandwidth on 1-14 cores. However, in Fig. 2a we see that the bandwidth is not fully saturated on 14 cores even for the case $n \times 1$. So our implementation partly seems to be limited by the in-core performance even for the memory-bound cases. This effect increases with the number of columns, respectively with the compute intensity. This indicates that our implementation is still sub-optimal. In addition, the simple Roofline model based on the number of floating point operations is too optimistic for this case because the TSQR algorithm includes data dependencies as well as costly sqrt operations. Overall we obtain more than 50% of the peak bandwidth for small numbers of columns. For the compute-



(a) Obtained memory bandwidth with our Q-less TSQR implementation.

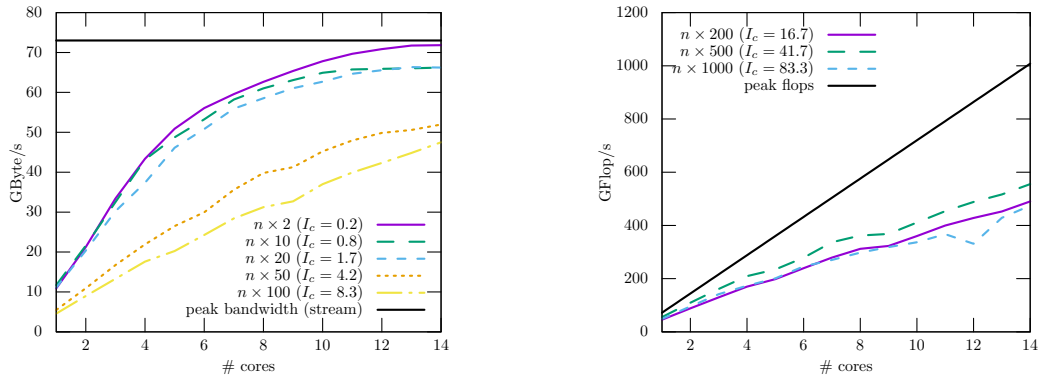


(b) Run-time for the QR decomposition (respectively a SVD) of a double precision $10^7 \times m$ matrix for $m = 1, \dots, 50$ with our Q-less TSQR implementation, Intel MKL 2020.3, and Trilinos 13.0.0.

Figure 3: Single socket performance of tall-skinny matrix decompositions for varying numbers of columns.

bound case ($m \geq 50$ on this hardware), we observe the expected linear scaling with the number of cores (see Fig. 2b). Our implementation achieves roughly 25% of the peak performance here, independent of the number of columns. So further code optimizations (such as loop blocking) could improve the performance for this case.

Fig. 3a shows the obtained bandwidth on a full socket and the Roofline limit depending on the number of columns m . The kink in the Roofline limit denotes the point where the operation (theoretically) becomes compute-bound. We see that the obtained bandwidth of our implementation decreases with the number of columns even in the memory-bound regime. However, our specialized TSQR implementation is still significantly faster than just calling some standard QR algorithm that is not optimized for tall-skinny matrices. This is illustrated by Fig. 3b. The comparison with MKL is fair concerning the hardware setting (single socket with 14 cores, no NUMA effects). However, it is unfair from the algorithmic point of view because we can directly discard Q and exploit the known memory layout whereas the MKL QR algorithm must work for all matrix shapes and any given memory layout and strides. We also show the run-time of the MKL SVD calculation for the same matrix dimensions. Calculating the singular values and the right singular vectors from the resulting R of the TSQR algorithm requires no significant additional time (SVD of $m \times m$ matrix with small m). In addition, we measured the run-time of the Trilinos [40] TSQR algorithm with the Trilinos Tpetra library on one MPI process per core. The Trilinos TSQR algorithm explicitly calculates the matrix Q and it does not seem to exploit SIMD parallelism: We only obtained scalar fused-multiply add instructions (FMA) instead of AVX512 (GCC 10.2 compiler with appropriate flags). Due to these two reasons, the Trilinos TSQR is still slower than our almost optimal Q-less TSQR implementation by more than a factor of 10. Overall, the QR trick with our Q-less TSQR implementation reduces the run-time of the SVD calculation by roughly a factor of 50 compared to just calling standard LAPACK (MKL) routines.



(a) Memory-bound case ($I_c \lesssim 11$) measured with $n = 10^7$.

(b) Compute-bound case ($I_c \gtrsim 11$) measured with $n = 5 \cdot 10^6$.

Figure 4: Single socket TSMM+reshape compared with the peak bandwidth respectively peak Flop/s.

5.1.2 Tall-skinny matrix-matrix multiplication (TSMM)

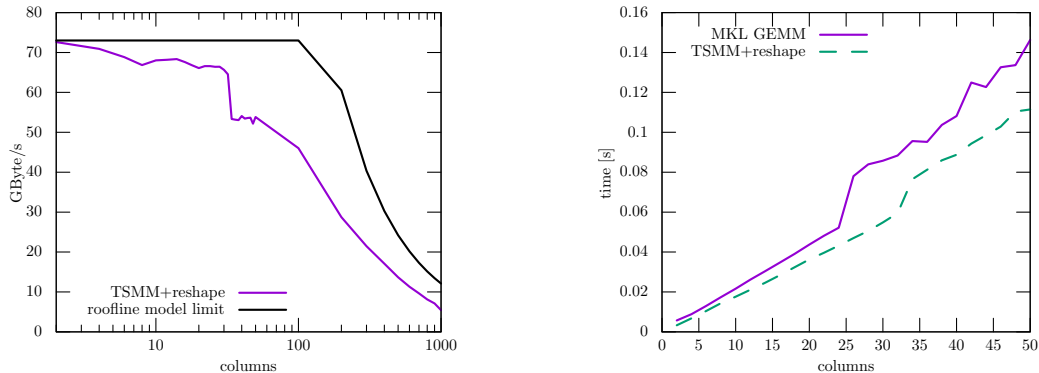
As analyzed in Section 4.1.2, the fused tall-skinny matrix-matrix multiplication and reshape is also memory-bound for m up to ~ 150 columns on the given hardware. Fig. 4a shows the obtained bandwidth for varying numbers of cores. We observe a saturation of the memory bandwidth for $m < 50$. For $m = 100$, we already see a linear scaling with the number of cores. For the compute-bound case, our implementation roughly obtains 50% of the peak performance (see Fig. 4b). This indicates that code optimizations might still slightly improve the performance for the compute-bound case. From Fig. 5a, we conclude that our TSMM implementation obtains a high fraction of the maximum possible bandwidth. Near the kink, the Roofline model is too optimistic because it assumes that data transfers and floating point operations overlap perfectly. Further insight could be obtained by a more sophisticated performance model such as the ECM (Execution-Cache-Memory) model, see [38]. For this operation, our implementation and the Intel MKL obtain roughly the same performance, as depicted in Fig. 5. In contrast to the MKL, our implementation exploits a special memory layout, which might explain the small differences in run-time. So the advantage of our TSMM implementation for the complete TT-SVD algorithm consists mainly in fusing the reshape operation, which ensures a suitable memory layout for all operations at no additional cost.

5.2 TT-SVD

In the following, we consider the complete TT-SVD algorithm and different variants and implementations of it. Fig. 6a illustrates the run-time of the TT-SVD algorithm in different software libraries. All cases show the run-time for decomposing a random double-precision 2^{27} tensor on a single CPU socket with 14 cores with a prescribed maximal TT-rank. For several of these libraries, we tested different variants and LAPACK back-ends [3, 25]. Here, we only report the timings for the fastest variant that we could find. We show results for the following libraries:

TSQR TT-SVD The implementation discussed in this paper.

ttpy A library written in Fortran and Python by the author of [34].



(a) Obtained memory bandwidth of our TSMM implementation.

(b) Run-time for the fused tall-skinny matrix-matrix multiplication of a double precision $10^7 \times m$ matrix with an $m \times \frac{m}{2}$ matrix for $m = 2, \dots, 50$.

Figure 5: Single socket performance of TSMM+reshape for varying numbers of columns.

t3f A library based on the TensorFlow framework [31].

TensorToolbox A Python library from the author of [8].

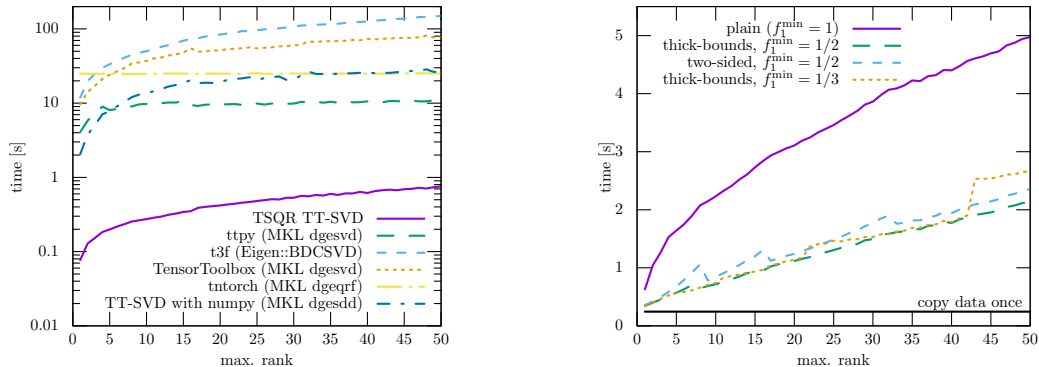
tntorch A library based on PyTorch [6].

TT-SVD with numpy Simple implementation in numpy [23] inspired by [18].

Both **ttpy** and **TensorToolbox** use the older (and in many cases slower) **dgesvd** routine for calculating SVD decompositions. Our classical TT-SVD implementation with **numpy** uses the newer LAPACK routine **dgesdd**. The **ttpy** library is still faster in many cases. The **t3f** library is based on TensorFlow, which is optimized for GPUs and uses the C++ Eigen library [21] as back-end on CPUs. However, only some routines in Eigen are parallelized for multi-core CPUs which explains why **t3f** is slow in this comparison. In contrast to all other variants, the run-time of the TT decomposition in **tntorch** is almost independent of the maximal TT-rank. **tntorch** does not implement the TT-SVD algorithm, but instead first constructs a tensor train of maximal rank, followed by a left-right orthogonalization step and TT rounding. The computationally costly part is the left-right orthogonalization step, which is based on QR decompositions whose size only depend on the size of the input tensor and not on the desired rank.

Our TSQR TT-SVD implementation is significantly faster than all other implementations for two reasons. First, there are multiple combinations of basic linear algebra building blocks that calculate the desired result. This is an example of the linear algebra mapping problem as discussed in [37]. Here, we choose a combination of building blocks (Q-less TSQR + multiplication with truncated right singular vectors) that leads to (almost) minimal data transfers. Second, common linear algebra software and algorithms are not optimized for avoiding data transfers. However, for the tall-skinny matrix operations required here, the data transfers determine the performance. For a detailed overview on communication avoiding linear algebra algorithms, see e.g. [5] and the references therein. An interesting discussion that distinguishes between the effects of reading and modifying data can be found in [9].

Fig. 6b shows the run-time for the different variants of the TSQR TT-SVD algorithm discussed in Section 4.2. This is the worst case run-time of the algorithm because we approximate a



(a) Different implementations of the classical TT-SVD algorithm for a 2^{27} tensor and our TSQR TT-SVD algorithm (without combining dimensions).

(b) Algorithmic variants of TSQR TT-SVD for a 2^{30} tensor with different prescribed reduction factors f_1^{\min} .

Figure 6: Single socket run-time of different TT-SVD algorithms for varying maximal TT-rank.

random input matrix and we only prescribe the maximal TT-rank. The parameter f_1^{\min} denotes the prescribed minimal reduction in size in the first step. For the plain case ($f_1^{\min} = 1$), there is no reduction in the data size in the first steps for $r_{\max} > 1$. In addition we also increase the first dimension for very small maximal rank to e.g. $n_1 \geq \max(fr_{\max}, 16)$. This reduces the run-time for very small TT-ranks (difference between plain and other variants for $r_{\max} = 1$). See Table 2 for some examples on resulting dimensions and TT-ranks. As expected, the plain variant is slower as it needs to transfer more data in the first iterations. For all cases with a prescribed reduction $f_1^{\min} < 1$, we observe roughly a linear scaling with the maximal TT-rank as predicted by the performance analysis for the compute-bound case. And for small ranks, the run-time is of the order of copying the data in memory. For our implementation the choice $f_1^{\min} = 1/2$ appears to be optimal even though the theoretical analysis indicates that a smaller f_1^{\min} could be beneficial. Increasing the prescribed reduction factor f_1^{\min} increases the number of columns of the matrices in the first step. This leads to more work and the obtained bandwidth of our TSQR implementation decreases (see Fig. 3a). The two-sided variant uses thick-bounds as well but it is always slower with our implementation.

The run-time of the individual steps of the algorithm are illustrated in Fig. 7. We clearly see the effect of combining multiple dimensions to obtain a reduction in the first step: The first TSQR and TSMM steps take longer but all subsequent steps are faster. The two-sided variant is only slower due to the additional transpose operation required in our implementation. Without the transpose operation, the two-sided variant would be slightly faster.

To check our estimates for the data transfer volume in (21) and the number of floating point operations in (25), we measured these quantities for several cases using CPU performance counters, see Table 3. We compare cases where the simple estimates with the global reduction factor \bar{f} fit well and we observe a good correlation with the measurements. Depending on the dimensions and the desired maximal rank, the reduction in the first step can differ from the following steps (see Table 2). For those cases, the equations based on a global reduction factor \bar{f} provide less accurate results.

In most of the experiments shown here, we use 2^d tensors for simplicity (as in the QTT format). If we increase the size of the individual dimensions, the compute intensity of the TSQR

case	r_{\max}	effective dim. (n_i)	TT-ranks (r_i)	reduction factors (f_i)
plain ($f_1^{\min} = 1$)	1	2, 2, ...	1, 1, ...	$\frac{1}{2}, \frac{1}{2}, \dots$
	5	2, 2, ...	2, 4, 5, 5, ...	1, 1, $\frac{5}{8}, \frac{1}{2}, \dots$
	7	2, 2, ...	2, 4, 7, 7, ...	1, 1, $\frac{7}{8}, \frac{1}{2}, \dots$
	16	2, 2, ...	2, 4, 8, 16, 16, ...	1, 1, 1, 1, $\frac{1}{2}, \dots$
thick-bounds ($f_1^{\min} = 1/2$)	1	16, 2, 2, ...	1, 1, ...	$\frac{1}{16}, \frac{1}{2}, \frac{1}{2}, \dots$
	5	16, 2, 2, ...	5, 5, ...	$\frac{5}{16}, \frac{1}{2}, \frac{1}{2}, \dots$
	7	16, 2, 2, ...	7, 7, ...	$\frac{7}{16}, \frac{1}{2}, \frac{1}{2}, \dots$
	16	32, 2, 2, ...	16, 16, ...	$\frac{1}{2}, \frac{1}{2}, \dots$
thick-bounds ($f_1^{\min} = 1/3$)	1	16, 2, 2, ...	1, 1, ...	$\frac{1}{16}, \frac{1}{2}, \frac{1}{2}, \dots$
	5	16, 2, 2, ...	5, 5, ...	$\frac{5}{16}, \frac{1}{2}, \frac{1}{2}, \dots$
	7	32, 2, 2, ...	7, 7, ...	$\frac{7}{32}, \frac{1}{2}, \frac{1}{2}, \dots$
	16	64, 2, 2, ...	16, 16, ...	$\frac{1}{4}, \frac{1}{2}, \frac{1}{2}, \dots$

Table 2: Examples for the resulting effective dimensions and TT-ranks for the different TT-SVD variants for a 2^d tensor.

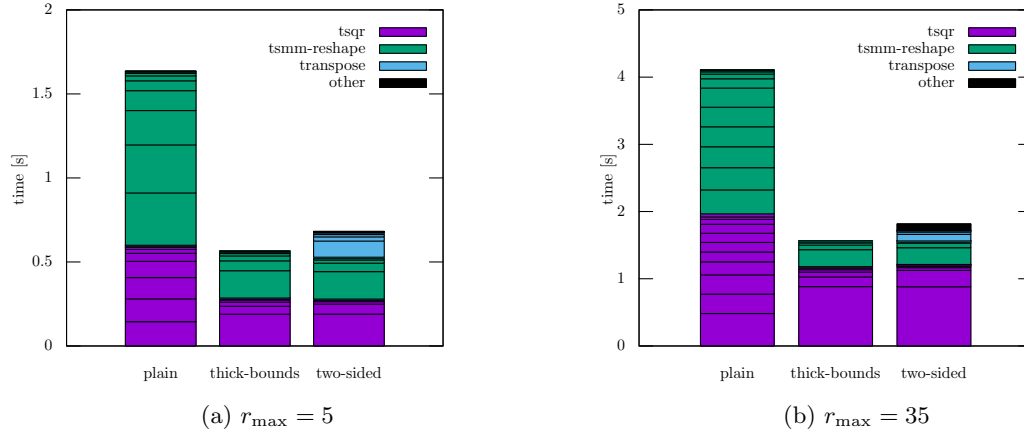


Figure 7: Timings for the building blocks in different TT-SVD variants. The thick-bounds and two-sided variants use the parameter $f_1^{\min} = 1/2$.

case	r_{\max}	operations [GFlop]	data transfers [GByte]
plain	1	14	43
thick-bounds	1	41	21
thick-bounds	31	417	43
estimate for $\bar{f} = 1/2$	1	13	43
estimate for $\bar{f} = 1/16$	1	39	19
estimate for $\bar{f} = 1/2$	31	399	43

Table 3: Measured and estimated number of floating point operations and data volume between the CPU and the main memory for the TSQR TT-SVD algorithm with a 2^{30} tensor in double precision. The measurements were performed with likwid-perfctr [39]. The estimates are based on (21) and (25).

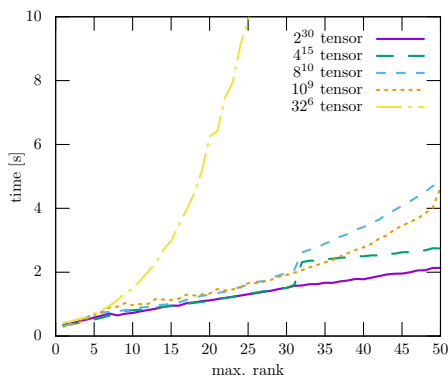


Figure 8: Timings for TSQR TT-SVD for varying dimensions on a single socket. Uses the thick-bounds variant with $f_1^{\min} = \frac{1}{2}$ where beneficial. The run-time for the case 32^6 continues to grow linearly with the maximal rank as expected for $r_{\max} > 20$.

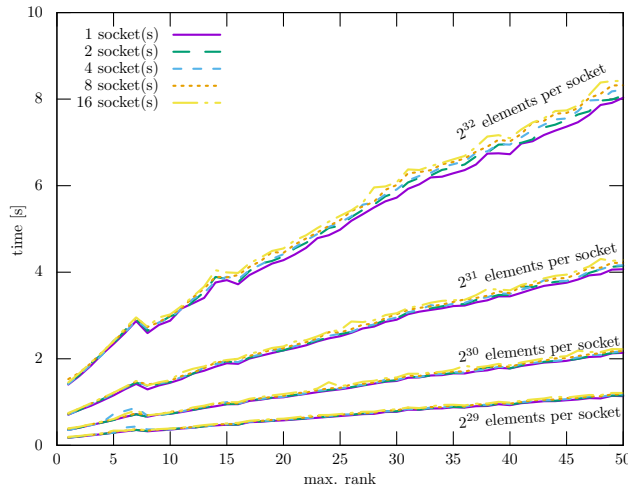


Figure 9: Timings for TSQR TT-SVD (thick-bounds variant with $f_1^{\min} = \frac{1}{2}$) for varying number of CPU sockets and nodes with 1 MPI process per socket. Each node has 4 sockets with 14 cores. The smallest case decomposes a 2^{29} tensor on a single socket of one node – the largest case a $2^{36} = 2^{32} \cdot 16$ tensor on 4 nodes.

TT-SVD algorithm increases. Fig. 8 visualizes the run-time for decomposing tensors of different dimensions with approximately the same total size. For very small maximal rank ($r_{\max} < 5$), all cases require similar run-time. For higher maximal ranks, the cases with a higher individual dimension become more costly. For $r_{\max} \geq 32$ there are some interesting deviations in the run-time from the expected linear growth. We can explain these deviations by the possible variants for combining dimensions in the thick-bounds algorithm: depending on r_{\max} and n_i there are only few discrete choices for the number of columns m of the first step. In particular, we obtain $m = 100$ for $r_{\max} = 10, \dots, 49$ for the 10^9 tensor but $m = 512$ for $r_{\max} = 32, \dots, 255$ for the 8^{10} tensor with a prescribed minimal reduction $f_1^{\min} = 1/2$. This results in a lower run-time for the 10^9 tensor as the first step is the most costly part of the algorithm. As expected, the run-time of the 32^6 case increases linearly with the maximal rank for $r_{\max} \geq 16$ and the run-time is significantly higher than for smaller dimensions as the actual reduction factors are small ($f_i \approx 1/32$).

Finally, we also tested a distributed variant of the TSQR TT-SVD algorithm using MPI. Fig. 9 shows weak scaling results for the variant $f_1^{\min} = 1/2$ and tensor dimensions from 2^{29} to 2^{36} (550 GByte in double precision) on up to 4 nodes with 4 sockets per node (total of 224 cores). The MPI processes only communicate for a global TSQR tree reduction of small $m \times m$ blocks where m is the number of columns of the tall-skinny matrix. Small operations (SVD decompositions of $m \times m$ matrices) are duplicated on all MPI processes. We observe a good weak scaling behavior with a small overhead of the MPI parallel variant compared to a single CPU socket. So the distributed variant allows us to tackle problems where the dense input tensor is too large for the memory of a single node, or where the input tensor is generated by a distributed program on a cluster.

6 Conclusion and future work

In this paper we analyzed the node-level performance of the tensor train SVD algorithm that calculates a low-rank approximation of some high-dimensional tensor. The results can also be transferred to other non-randomized high-order SVD algorithms. We considered the case where the input tensor is large and dense, but not too large to be processed completely i.e., read from main memory or disk. The theoretical minimal run-time depends on the desired accuracy of the approximation. For small tensor train ranks (low accuracy), the algorithm is memory-bound and the ideal run-time on current hardware is approximately twice the time required for reading the data (transfer it from the memory to the CPU). For larger tensor train ranks (higher accuracy), the algorithm becomes compute-bound and the ideal run-time increases linearly with the maximal TT-rank. We presented different variants of the TT-SVD algorithm. To reduce the computational complexity, these variants start with the calculation of the TT-cores at the boundaries of the tensor train and reduce the data size in each step. The key ingredient is a Q-less tall-skinny QR decomposition based on Householder reflections that handles rank-deficient matrices without pivoting by clever use of floating point arithmetic. We performed numerical experiments with 2^d tensors of size up to 550 GByte ($d = 36$) on up to 4 nodes (224 cores) of a small HPC cluster. Our hybrid-parallel (MPI+OpenMP) TT-SVD implementation achieves almost optimal run-time for small ranks and about 25% peak performance for larger TT-ranks. On a single CPU socket, our implementation is about $50\times$ faster compared to other common TT-SVD implementations in existing software libraries. Our estimate for the lower bound of the run-time is reading the data twice from main memory. This also indicates when it might be beneficial to switch to randomized HOSVD algorithms that can circumvent this lower bound by not considering all data.

For future work, we see three interesting research directions: First, in our numerical experiments, we use random input data and prescribe the TT-ranks. In real applications, usually a certain truncation accuracy is prescribed instead, and the TT-ranks depend on the desired accuracy and characteristics of the input data. For optimal performance one needs to combine, rearrange or split dimensions based on some heuristic such that the first step leads to a sufficient reduction in data size. Second, our algorithm only works well for dense input data. Handling sparse input data efficiently is more challenging as the reduction in dimensions in each step does not necessarily lead to smaller data for the sparse case. And finally, it would be interesting to analyze the performance of randomized HOSVD algorithms and to deduce lower bounds for their run-time on current hardware.

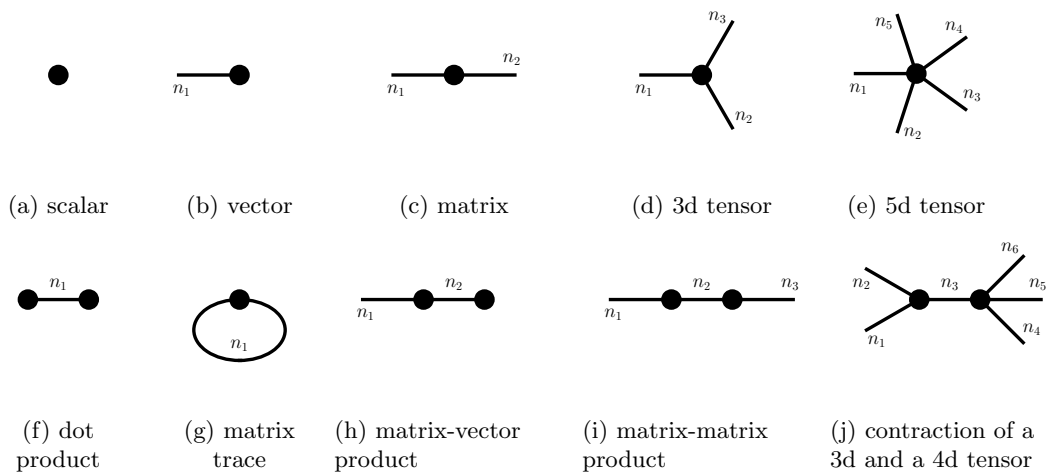
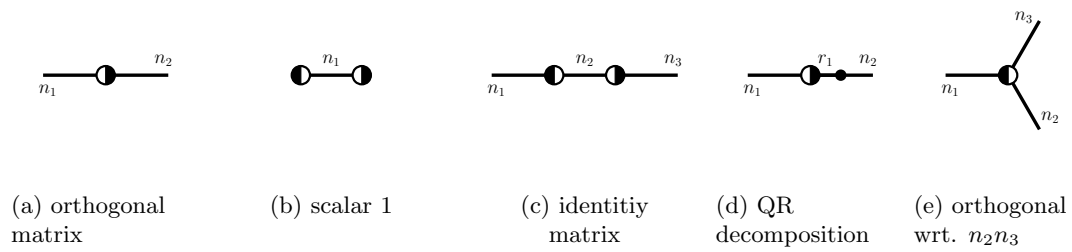


Figure 10: Simple tensor network diagrams.

A Tensor network diagram notation

A tensor network diagram is a graph where each node depicts a tensor. The number of outgoing edges determines the number of dimensions of the tensor and an edge between two nodes specifies a contraction (generalization of a matrix-matrix product) of the given dimension, see Fig. 10. This notation allows us to describe tensor decompositions, e.g. a decomposition of a 5-dimensional tensor into a contraction of a 3- and a 4-dimensional tensor (see last graph in Fig. 10). In the tensor network diagram, a half-filled circle denotes a tensor that is orthonormal with respect to the dimensions attached to the white half, see Fig. 11. Fig. 11a shows an orthogonal matrix for $n_1 = n_2$. For $n_1 > n_2$, the matrix has orthogonal columns with norm one. The diagrams in Fig. 11f show the steps of an orthogonalization algorithm in a tensor network.



(f) Left-orthogonalization algorithm: calculate a QR decomposition of the left tensor, contract R and the right tensor, calculate a QR decomposition of the right tensor, ...

Figure 11: Orthogonal matrices and decompositions in a tensor network diagram.

References

- [1] I. AFFLECK, *Large- n limit of $SU(n)$ quantum "spin" chains*, Physical Review Letters, 54 (1985), pp. 966–969, <https://doi.org/10.1103/PhysRevLett.54.966>.
- [2] I. AFFLECK, T. KENNEDY, E. H. LIEB, AND H. TASAKI, *Rigorous results on valence-bond ground states in antiferromagnets*, Physical Review Letters, 59 (1987), pp. 799–802, <https://doi.org/10.1103/PhysRevLett.59.799>.
- [3] E. ANDERSON, Z. BAI, C. BISCHOF, L. S. BLACKFORD, J. DEMMEL, J. DONGARRA, J. D. CROZ, A. GREENBAUM, S. HAMMARLING, A. MCKENNEY, AND D. SORENSEN, *LAPACK Users' Guide*, Society for Industrial and Applied Mathematics, 1999, <https://doi.org/10.1137/1.9780898719604>.
- [4] J. BALLANI, L. GRASEDYCK, AND M. KLUGE, *Black box approximation of tensors in hierarchical Tucker format*, Linear Algebra and Its Applications, 438 (2013), pp. 639–657, <https://doi.org/10.1016/j.laa.2011.08.010>.
- [5] G. BALLARD, E. CARSON, J. DEMMEL, M. HOEMMEN, N. KNIGHT, AND O. SCHWARTZ, *Communication lower bounds and optimal algorithms for numerical linear algebra*, Acta Numerica, 23 (2014), pp. 1–155, <https://doi.org/10.1017/s0962492914000038>.
- [6] R. BALLESTER-RIPOLL, *ntorch - Tensor Network Learning with PyTorch*. <https://ntorch.readthedocs.io>, 2019. Revision 8c81a1cb.
- [7] M. W. BERRY, S. A. PULATOVA, AND G. W. STEWART, *Algorithm 844*, ACM Transactions on Mathematical Software, 31 (2005), pp. 252–269, <https://doi.org/10.1145/1067967.1067972>.
- [8] D. BIGONI, A. P. ENGSIG-KARUP, AND Y. M. MARZOUK, *Spectral tensor-train decomposition*, SIAM Journal on Scientific Computing, 38 (2016), pp. A2405–A2439, <https://doi.org/10.1137/15m1036919>.
- [9] E. CARSON, J. DEMMEL, L. GRIGORI, N. KNIGHT, P. KOANANTAKOOL, O. SCHWARTZ, AND H. V. SIMHADRI, *Write-avoiding algorithms*, in 2016 IEEE International Parallel and Distributed Processing Symposium (IPDPS), IEEE, may 2016, pp. 648–658, <https://doi.org/10.1109/ipdps.2016.114>.
- [10] C. CHEN, K. BATSELIER, C.-Y. KO, AND N. WONG, *A support tensor train machine*, in 2019 International Joint Conference on Neural Networks (IJCNN), IEEE, Jul 2019, <https://doi.org/10.1109/ijcnn.2019.8851985>.
- [11] C. CHEN, K. BATSELIER, W. YU, AND N. WONG, *Kernelized support tensor train machines*, (2020), <https://arxiv.org/abs/2001.00360v1>.
- [12] P. G. CONSTANTINE, D. F. GLEICH, Y. HOU, AND J. TEMPLETON, *Model reduction with MapReduce-enabled tall and skinny singular value decomposition*, SIAM Journal on Scientific Computing, 36 (2014), pp. S166–S191, <https://doi.org/10.1137/130925219>.
- [13] H. A. DAAS, G. BALLARD, AND P. BENNER, *Parallel algorithms for tensor train arithmetic*, (2020), <https://arxiv.org/abs/2011.06532v1>.
- [14] J. DEMMEL, L. GRIGORI, M. HOEMMEN, AND J. LANGOU, *Communication-optimal parallel and sequential QR and LU factorizations*, SIAM Journal on Scientific Computing, 34 (2012), pp. A206–A239, <https://doi.org/10.1137/080731992>.

- [15] J. W. DEMMEL, L. GRIGORI, M. GU, AND H. XIANG, *Communication avoiding rank revealing QR factorization with column pivoting*, SIAM Journal on Matrix Analysis and Applications, 36 (2015), pp. 55–89, <https://doi.org/10.1137/13092157x>.
- [16] S. DOLGOV AND B. KHOROMSKIJ, *Two-level QTT-tucker format for optimized tensor calculus*, SIAM Journal on Matrix Analysis and Applications, 34 (2013), pp. 593–623, <https://doi.org/10.1137/120882597>.
- [17] H.-Y. FAN, L. ZHANG, E. W. CHU, AND Y. WEI, *Q-less QR decomposition in inner product spaces*, Linear Algebra and Its Applications, 491 (2016), pp. 292–316, <https://doi.org/10.1016/j.laa.2015.08.035>.
- [18] P. GELSS, S. KLUS, M. SCHERER, F. NÜSKE, AND M. LÜCKE, *Scikit-TT tensor-train computations in python*. https://github.com/PGelss/scikit_tt, 2019. Revision 1dfd64a.
- [19] L. GRASEDYCK AND W. HACKBUSCH, *An introduction to hierarchical (h-) rank and TT-rank of tensors with examples*, Computational Methods in Applied Mathematics, 11 (2011), pp. 291–304, <https://doi.org/10.2478/cmam-2011-0016>.
- [20] L. GRASEDYCK, D. KRESSNER, AND C. TOBLER, *A literature survey of low-rank tensor approximation techniques*, GAMM Mitteilungen, 36 (2013), pp. 53–78, <https://doi.org/10.1002/gamm.201310004>.
- [21] G. GUENNEBAUD, B. JACOB, ET AL., *Eigen v3*. <http://eigen.tuxfamily.org>, 2010. Version 3.3.9.
- [22] G. HAGER AND G. WELLEIN, *Introduction to High Performance Computing for Scientists and Engineers*, CRC Press, jul 2010, <https://doi.org/10.1201/ebk1439811924>.
- [23] C. R. HARRIS, K. J. MILLMAN, S. J. VAN DER WALT, R. GOMMERS, P. VIRTANEN, D. COURNAPEAU, E. WIESER, J. TAYLOR, S. BERG, N. J. SMITH, R. KERN, M. PICUS, S. HOYER, M. H. VAN KERKWIJK, M. BRETT, A. HALDANE, J. F. DEL RÍO, M. WIEBE, P. PETERSON, P. GÉRARD-MARCHANT, K. SHEPPARD, T. REDDY, W. WECKESSER, H. ABBASI, C. GOHLKE, AND T. E. OLIPHANT, *Array programming with NumPy*, Nature, 585 (2020), pp. 357–362, <https://doi.org/10.1038/s41586-020-2649-2>.
- [24] A. S. HOUSEHOLDER, *Unitary triangularization of a nonsymmetric matrix*, Journal of the ACM, 5 (1958), pp. 339–342, <https://doi.org/10.1145/320941.320947>.
- [25] INTEL, *Math kernel library (mkl)*. <https://software.intel.com/mkl>. Version 2020.3.
- [26] B. N. KHOROMSKIJ, *$O(d \log N)$ -quantics approximation of n -d tensors in high-dimensional numerical modeling*, Constructive Approximation, 34 (2011), pp. 257–280, <https://doi.org/10.1007/s00365-011-9131-1>.
- [27] S. KLUS AND P. GELSS, *Tensor-based algorithms for image classification*, Algorithms, 12 (2019), p. 240, <https://doi.org/10.3390/a12110240>.
- [28] T. G. KOLDA AND D. HONG, *Stochastic gradients for large-scale tensor decomposition*, SIAM Journal on Mathematics of Data Science, 2 (2020), pp. 1066–1095, <https://doi.org/10.1137/19m1266265>.
- [29] K. KOUR, S. DOLGOV, M. STOLL, AND P. BENNER, *Efficient structure-preserving support tensor train machine*, <https://arxiv.org/abs/2002.05079v2>.

- [30] B. W. LARSEN AND T. G. KOLDA, *Practical leverage-based sampling for low-rank tensor decomposition*, <https://arxiv.org/abs/2006.16438v2>.
- [31] A. NOVIKOV, P. IZMAILOV, V. KHRULKOV, M. FIGURNOV, AND I. OSELEDETS, *Tensor Train Decomposition on TensorFlow (T3F)*, Journal of Machine Learning Research, 21 (2020), pp. 1–7, <http://jmlr.org/papers/v21/18-008.html>.
- [32] I. OSELEDETS AND E. TYRTYSHNIKOV, *TT-cross approximation for multidimensional arrays*, Linear Algebra and its Applications, 432 (2010), pp. 70–88, <https://doi.org/10.1016/j.laa.2009.07.024>.
- [33] I. V. OSELEDETS, *A new tensor decomposition*, Doklady Mathematics, 80 (2009), pp. 495–496, <https://doi.org/10.1134/S1064562409040115>.
- [34] I. V. OSELEDETS, *Tensor-Train Decomposition*, SIAM Journal on Scientific Computing, 33 (2011), pp. 2295–2317, <https://doi.org/10.1137/090752286>.
- [35] I. V. OSELEDETS AND E. E. TYRTYSHNIKOV, *Breaking the curse of dimensionality, or how to use svd in many dimensions*, SIAM Journal on Scientific Computing, 31 (2009), pp. 3744–3759, <https://doi.org/10.1137/090748330>.
- [36] R. PENROSE, *Applications of negative dimensional tensors*, Combinatorial Mathematics and its Applications, (1971), pp. 221–244.
- [37] C. PSARRAS, H. BARTHELS, AND P. BIENTINESI, *The linear algebra mapping problem*, <https://arxiv.org/abs/1911.09421v1>.
- [38] H. STENGEL, J. TREIBIG, G. HAGER, AND G. WELLEIN, *Quantifying performance bottlenecks of stencil computations using the execution-cache-memory model*, in Proceedings of the 29th ACM on International Conference on Supercomputing - ICS '15, ACM Press, 2015, <https://doi.org/10.1145/2751205.2751240>.
- [39] J. TREIBIG, G. HAGER, AND G. WELLEIN, *LIKWID: A lightweight performance-oriented tool suite for x86 multicore environments*, in 2010 39th International Conference on Parallel Processing Workshops, IEEE, Sept. 2010, <https://doi.org/10.1109/icppw.2010.38>.
- [40] T. TRILINOS PROJECT TEAM, *The Trilinos Project Website*. <https://trilinos.github.io>, 2020. Accessed May 22, 2020.
- [41] F. VERSTRAETE AND J. I. CIRAC, *Matrix product states represent ground states faithfully*, Physical Review B, 73 (2006), p. 094423, <https://doi.org/10.1103/PhysRevB.73.094423>.
- [42] S. R. WHITE, *Density matrix formulation for quantum renormalization groups*, Physical Review Letters, 69 (1992), pp. 2863–2866, <https://doi.org/10.1103/PhysRevLett.69.2863>.
- [43] S. WILLIAMS, A. WATERMAN, AND D. PATTERSON, *Roofline: An insightful visual performance model for multicore architectures*, Communications of the ACM, 52 (2009), pp. 65–76, <https://doi.org/10.1145/1498765.1498785>.